Hardware Testbed for Sidelink Transmission of 5G Waveforms without Synchronization

David Garcia-Roger, Josue Flores de Valgas, Jose F. Monserrat, N. Cardona
Universitat Politècnica de València, iTEAM Research Institute
Valencia, Spain
Email: {dagarro,joflode1,jomondel,ncardona}@iteam.upv.es

Nicolo Incardona
Politecnico di Milano
Milano, Italy
Email: nicolo.incardona@mail.polimi.it

***Abstract*—This paper details a hardware testbed conceived for studying the impact of the lack of synchronism between transmitters on several 5G waveform candidates, which is of special relevance for car-to-car communications. The experimental results show that a proper fitting of waveforms in a software-defined platform would permit increasing the range of communication between cars without peer-to-peer synchronization, paving the way for the real development of collision avoidance messages.**

I. Introduction

IEEE 802.11p, also known as wireless access in the vehicular environment (WAVE), is an amendment to the IEEE 802.11 standard that extends its applicability to vehicular environments, including short-range communications for data exchange between vehicles (V2V) and between vehicles and the roadside infrastructure. IEEE 802.11p is based on orthogonal frequency-division multiplexing (OFDM) [1], being its multiple access counterpart, OFDMA, widely used to divide the spectrum in multiple and orthogonal parallel sub-bands, as it happens in long term evolution (LTE) technology [2]. However, as it turns out, the orthogonality property of OFDMA is only verified under ideal conditions, that is to say, under perfect frequency synchronization and precise time alignment during the cyclic prefix (CP). This issue imposes critical requirements, in such a way that, in order not to introduce inter-carrier interference (ICI) or inter-symbol interference (ISI), the terminals should be prevented from transmitting if a central entity does not verify that both time and frequency alignment are being respected. However, in the current design of LTE-Vehicle (LTE-V) the synchronization requirements are becoming a crucial issue. For example, while vehicles may be synchronized with elements of the roadside infrastructure (i.e. base stations), it is not expected that the synchronism between vehicles in a V2V sidelink communication scenario would be supported by such elements; thus specific synchronization signals are now under discussion for the support of this direct V2V communication. Moreover, the concept of timing advance (TA) may not be reused because it only assists in the determination of the distance to a common element (the base station) and is useless when determining the distance between two vehicles with varying relative distances. Consequently, it is of the utmost benefit to assess alternatives to OFDM, which should be able to tolerate a lower degree of synchronization without introducing additional ICI or ISI.

The filter bank multi-carrier (FBMC) [3] and the universal filtered OFDM (UF-OFDM), also known as universal filtered multi-carrier (UFMC) [4], modulation schemes are two of the alternative fifth-generation (5G) waveform candidates currently under consideration for designing a multicarrier physical (PHY) layer. Like OFDM, FBMC and UF-OFDM schemes segment the spectrum into multiple orthogonal sub-bands. However, unlike OFDM, FBMC performs a per-subcarrier filtering and UF-OFDM applies a filter to blocks of subcarriers. As a result, with FBMC and UF-OFDM the sidelobes are attenuated and thus the ICI and ISI issues are less critical than with OFDM for transmissions not perfectly synchronized.

5G waveform candidates have been subject of research efforts for several years, but so far mainly from the theoretical viewpoint, with only a few experimental testbeds [5]–[7], which do not address the synchronization requirements of the studied waveforms. This paper explains the usefulness of the proposed hardware testbed in checking the feasibility of each 5G waveform candidate for sidelink communications, and collects the results of evaluating the impact of the lack of synchronization and MIMO performance.

The remaining sections of the paper are structured as follows. Section II describes the waveforms implemented, briefly introducing OFDM, FBMC, and UF-OFDM implementations. Section III explains the V2V scenario studied in the testbed. Section IV gives an overview of the experimental hardware testbed, whereas Section V provides additional details about its software components and Section VI presents the measurement results. Finally, Section VII draws the main conclusions of this work.

II. Waveforms under Study

A. OFDM

A transmitter implementing the OFDM waveform uses a baseband constellation mapper to map a bit stream to a QPSK or QAM symbol called X. The symbol stream then passes through a serial-to-parallel converter to form a set of N parallel QAM symbols $X[0], X[1], \ldots, X[N-1]$ representing the symbols transmitted at each subcarrier. By modulating these symbols with the inverse fast Fourier transform (IFFT) at the transmitting side, a discrete baseband OFDM symbol

can be generated, which can be written as

$$x[n] = \mathcal{F}^{-1}\{X[i]\} = \frac{1}{\sqrt{N}} \sum_{i=0}^{N-1} X[i] e^{j\frac{2\pi}{N}ni}, 0 \leq n \leq N-1, \quad (1)$$

where N is the number of subcarriers, and $X[i]$ is the complex symbol transmitted on the i-th subcarrier.

The symbol may be obtained at the receiver side using the fast Fourier transform (FFT). Assuming perfect reconstruction, the recovered signal is

$$\hat{X}[i] = \mathcal{F}\{x[n]\} = \frac{1}{\sqrt{N}} \sum_{n=0}^{N-1} x[n] e^{j\frac{-2\pi}{N}ni}, 0 \leq i \leq N-1. \quad (2)$$

B. OQAM/FBMC

Multicarrier with offset QAM (OQAM), also known as staggered multitone (SMT) FBMC is chosen because of its maximum spectral efficiency [3]. OQAM/FBMC allows subcarrier bands that are maximally overlapped and minimally spaced (the carrier spacing is equal to the symbol rate).

A transmitter implementing the OQAM/FBMC waveform uses a baseband constellation mapper to map a bit stream to an OQAM symbol on the i-th carrier of the m-th frame denoted by $X_m[i]$. By applying OQAM, the transmitter splits the symbols into their real and imaginary parts and modulates the staggered in-phase and quadrature components by half a symbol period. In addition, to keep up the bit rate, the FFT is run at twice the rate as in OFDM, with real and imaginary symbols alternating both in time and frequency axis. In contrast to OFDM, OQAM/FBMC is not orthogonal with respect to the complex plane, and each subcarrier introduces interference to its neighboring subcarriers; the use of OQAM allows this interference to be easily cancelled at the receiver by ignoring the part of the received symbol not carrying data.

FBMC applies a filtering functionality on a per subcarrier basis by means of a prototype filter (called so because the other filters are derived from it through frequency shifts). Prototype filters are characterized by the overlapping factor K, which is the number of multicarrier symbols which overlap in the time domain. Generally, K is an integer number, the amount of frequency coefficients which are introduced between the FFT filter coefficients in the frequency domain. Despite the overlapping, prototype filters are designed so as to transmit data in such a manner that no ISI occurs. In the testbed, the prototype filter applied is based on the frequency domain coefficients provided by [8] which are the same ones used by the FP7-PHYDIAS project [9]. With this prototype filter, a filter bank of the system is obtained via frequency shifts. Note that subcarriers with odd or even indexes do not overlap; only the neighbor subcarriers have influence in a certain subcarrier.

After the serial-to-parallel conversion at the transmitter, the OQAM symbols $X_m[i]$ are converted to the time domain by means of an IFFT, obtaining the output $x_m[n]$,

$$x_m[n] = \mathcal{F}^{-1}\{X_m[i]\} = \frac{1}{\sqrt{N}} \sum_{i=0}^{N-1} X_m[i] e^{j2\pi ni/N}. \quad (3)$$

The prototype filter is applied to these symbols before transmitting. To that effect, $x_m[n]$ is duplicated K times and then multiplied with the impulse response of the prototype filter. Each filtered frame symbol $y_m[n]$ is

$$y_m[n] = p[n] x_m[n \bmod N], \quad (4)$$

where $p[n]$ is the impulse response of length $L_p = NK$ of the prototype filter (given by applying the IFFT to the frequency response of the prototype filter).

All the filtered frame symbols must be shifted by half a symbol period $N/2$, obtaining the final transmitted signal $y[n]$,

$$y[n] = \sum_{m=1}^{K} y_m \Big[n - \frac{m-1}{2} N \Big]. \quad (5)$$

The shift extends the total length of y_n to $L_p + N(K-1)/2 = N(3K-1)/2$ samples. Long typical filter lengths of four times the symbol length are used because the frequency response of the filter needs to be rather tight. In turn, long ramp up and ramp down areas are required in case of bursty data transmissions. Both the fact that subcarriers are interferring into the subcarriers of their neighborhood, and the need for long filters cause various issues, especially if practical aspects of programming such waveform on a hardware testbed are considered.

The received signal $r[n]$ is divided into K frames and the prototype filter is applied to each frame. Note that the m-th frame verifies that $r_m[n] = r[n + \frac{m-1}{2} N]$. Therefore, by multiplying the m-th frame with the impulse response of the prototype filter, the following is obtained:

$$s_m[n] = p[n] r_m[n]. \quad (6)$$

The K symbols must be reassembled again into one symbol, denoted by $\hat{s}_m[n]$,

$$\hat{s}_m[n] = \sum_{k=0}^{K-1} s_m[n + kN], n = 0, 1, \ldots, N-1. \quad (7)$$

note that at the transmitter the symbol after the IFFT was originally duplicated K times. At this point, an FFT operation is applied to the symbol $\hat{s}_m[n]$, frame by frame, rebuilding the OQAM symbol $\hat{X}_m[i]$,

$$\hat{X}_m[i] = \mathcal{F}\{\hat{s}_m[n]\} = \frac{1}{\sqrt{N}} \sum_{n=0}^{N-1} \hat{s}_m[n] e^{-j2\pi ni/N}. \quad (8)$$

C. UF-OFDM

UF-OFDM may be considered a generalization of FBMC and OFDM. While FBMC filters at the subcarrier level and OFDM filters the entire band, UF-OFDM filters blocks of subcarriers (called sub-bands). So the entire bandwidth is divided into B sub-bands. Each sub-band may be allocated with n_k consecutive subcarriers, i.e. a sub-band may be considered like the physical resource block (PRB) concept of

LTE. With an N-point IFFT operation, and filling only the corresponding subcarriers, the frequency domain signal of the k-th sub-band, X_k, is transformed into the time domain as x_k. Then, this output signal is filtered by a finite impulse response (FIR) filter f_k of length L adapted to the k-th sub-band.

The filtering process results in a signal of length of $N+L-1$ because of the linear convolution between x_k and f_k. Then, all the filtered sub-band signals y_k are added together and transmitted, resulting in $\sum_{k=1}^{B} y_k$.

At the receiver, FFT-based detection is used to transform the received time domain signal into the frequency domain. Since the UF-OFDM symbol has length $N + L - 1$, zero-padding is needed to perform the $2N$-point FFT. The estimated symbol $\hat{X}[i]$ is derived from this $2N$-point FFT by taking only the even subcarriers, since odd subcarriers contain interference from all data symbols.

The classical cyclic prefix OFMC (CP-OFDM) is a special case of UF-OFDM with $L = 1$. Within a single sub-band, spectral properties for UF-OFDM are alike filtered OFDM, while different sub-bands are spectrally separated as FBMC separates single subcarriers. UF-OFDM does not require a cyclic prefix but may use it to further improve ISI protection. The filter length depends on the sub-band width. Values of 12 for the number of subcarriers combined into a single sub-band are typical, which corresponds with the LTE numerology for a PRB. Requiring for UF-OFDM that filter lengths be in the range of the CP is also typical, resulting in about 7% overhead.

III. V2V Scenario

This paper studies the effect of timing offset in OFDM, OQAM/FBMC, and UF-OFDM systems with respect to the sidelink three-user scenario depicted in Figure 1. As shown, the three vehicles are synchronized with respect to the base station via an ongoing closed-loop TA control enforced for each user in the uplink, thus anticipating the transmission so as to achieve perfect synchronization at the base station. TA is calculated as $\text{TA} = 2d/c$, being d the distance in meters between the base station and the vehicle and c the speed of light. In addition, if opportunistic sidelink communications are allowed, vehicles are free to transmit data between them at will. Under such conditions, time-aligning each user before the transmission can start, is unacceptable, and thus supporting multiple concurrent V2V transmissions renders impossible for vehicles to be perfectly synchronized between them. In fact, asynchronous operation may be necessary to reach an acceptable level of spectral efficiency.

This paper assumes that vehicles lack a dedicated synchronization mechanism between them, only synchronizing with the base station and using the same TA for their sidelink communications. In Figure 1, if car #1 and car #2 do not modify their TA, then the timing offset experienced at car #2 is $\text{TO} = \text{TA}_1 - \text{TA}_2 + (d_3/c)$. Sidelink communication opportunities distributed in frequency (and/or time) mapped into adjacent frequency resources (and/or consecutive symbols) produce timing offsets that will be perceived by the receiver as multiuser interference.

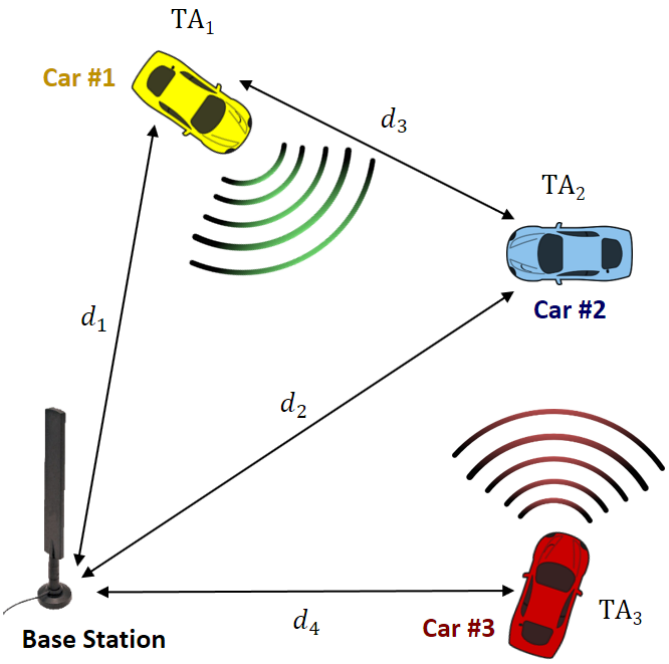

Fig. 1. V2V case scenario.

Previous work has evaluated the impact of timing synchronization for OFDM systems (analytically [10], or jointly with simulations [11]); for OQAM/FBMC (either mathematically [12], or combining analytical evaluation and numerical simulations [13], [14]; and for UF-OFDM (analysis and simulation [15]). Moreover, previous comparisons between waveforms have been done, again via numerical analysis and simulation: examining OFDM and FBMC [16], and studying OFDM, FBMC and UF-OFDM (among others) [17]. This paper complements the state of the art by assessing the impact of the timing offset by means of a hardware platform.

IV. Hardware Testbed

The hardware testbed is shown in Figure 2. It consists of three WARP v3 kit boards by Mango Communications [18]. Two of them are configured as transmitters and the other one as receiver.

The WARP v3 kit board is built around a Xilinx Virtex-6 LX240T field programmable gate array (FPGA) for the real-time transmission and reception of waveforms. Each of the three boards in the hardware testbed has access to four MAX2829-based radio interfaces with a 2.4/5 GHz transceiver of up to 40 MHz of RF bandwidth, and up to 20 dBm of transmission power. Each radio interface implements a full digital-to-RF transceiver chain; the conversion between the analog and digital domains is performed by an Analog Devices AD9963, and the conversion between baseband and RF is performad by a Maxim MAX2829.

For the communication with the boards, a computer with the 64-bit version of Windows 8.1 Enterprise installed on a two core 2.4 GHz processor with 4 GB of RAM is running MATLAB 2015b. The computer has a dedicated Gigabit

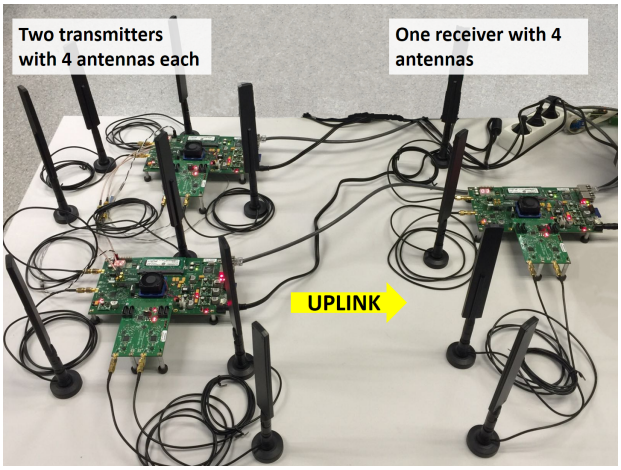

Fig. 2. 5G Waveforms Hardware Testbed.

Ethernet PCI-E NIC. The three WARP v3 kits are connected to each other and to the computer through the 1 Gigabit-Ethernet LAN ports of a TP-LINK TL-WR1043ND router.

V. Software-defined Radio Programming

The software developed on the hardware testbed generates an IEEE 802.11p frame consisting of three different fields: PLCP preamble, signal and multiple data, as shown in Figure 3. The PLCP preamble consists of a short (STS) and a long training sequence (LTS). The STS is a repetition of 10 equal short symbols of length 16 samples. The LTS comprises 2 identical sequences, of length 64 samples each, preceded by a 32-sample guard interval (GI). The synchronization process is split into a coarse timing offset and carrier frequency offset (CFO) estimation based on the LTS, followed by a fine estimation. The coarse TO estimation is accomplished with the algorithm in [19], currently a standard algorithm in OFDM systems. This delay-and-correlate algorithm exploits the periodicity of the training symbols. The coarse CFO estimation is performed with the correlation algorithm in [19]. After this coarse estimation, subsequent samples are multiplied by the CFO error estimates. After that, the program obtains an exact starting point at the first sample of the first LTS, which would be critical for the decoding process involving the FFT operation, moreover this starting point is useful because the LTS is also needed for channel estimation. This is achieved with cross-correlation or matched filter method, which correlates a local stored STS symbol with an already frequency-synchronized received signal. The output of the LTS correlator is a peak arising at the end of each of the two LTS symbols. The correlator implemented is a *SignSign* [20]. Fine carrier frequency offset estimation is performed with the aid of four pilot carriers. Finally, the data field contains multiple payload symbols carried by the waveforms analyzed in this paper. Note that the hardware testbed performs synchronization since the asynchronous situations are forced in a controlled manner by adding a certain shift into the signal samples.

TABLE I
Key 802.11p PHY layer parameters used

Parameters	IEEE 802.11p
FFT size	64
Total subcarriers	52
Data subcarriers	48
Pilot subcarriers	4
Symbol duration	8 µs
Guard interval	1.6 µs
FFT period	6.4 µs
Preamble Duration	32 µs
Subcarrier frequency spacing	0.156 25 MHz
Channel bandwidth	10 MHz
Band	5.9 GHz

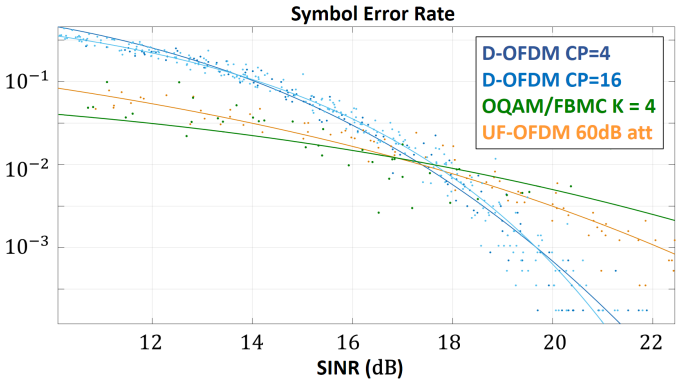

Fig. 4. Symbol error rate with respect to the signal-to-interference-plus-noise ratio.

VI. Performance Results

In this section, we compare the performance of the studied waveforms. A total number of 1000 measurements per waveform have been performed using the PHY layer parameters of IEEE 802.11p shown in Table I. In each case, the values of CP (OFDM), the overlap factor K (OQAM/FBMC), and sidelobe attenuation (UF-OFDM) are explicitly stated in the figures. The modulation used is 16-QAM. Note that we refer in the legends to dynamic OFDM (D-OFDM) to stress that, in this solution, CP can be modified dynamically to adapt to the different timing offsets.

The first results assume perfect synchronization between a transmitter and the base station in a SISO case. Figure 4 shows the symbol error rate with respect to the signal-to-interference-plus-noise (SINR) ratio. As shown in the figure, D-OFDM behaves better than OQAM/FBMC and UF-OFDM for higher values of SINR while the opposite is true for lower values. Figure 5 shows the throughput counterpart. As shown, while OQAM/FBMC and UF-OFDM achieve near 100% throughput, in the OFDM case the longer the CP the lower the throughput, because of the impact of the reduced spectral efficiency.

Next, the hardware testbed is used to mimic the sidelink communication scenario of Figure 1, where car #1 and car #3

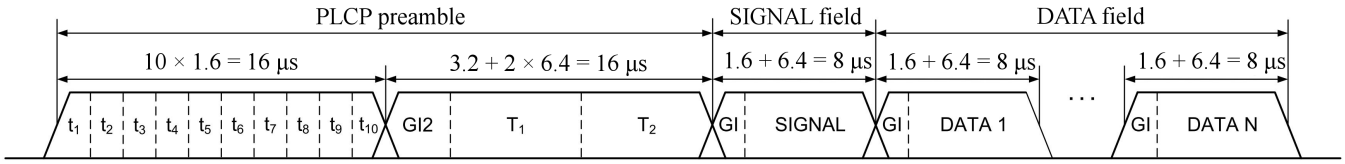

Fig. 3. IEEE 802.11p physical layer protocol data units (PPDU) frame.

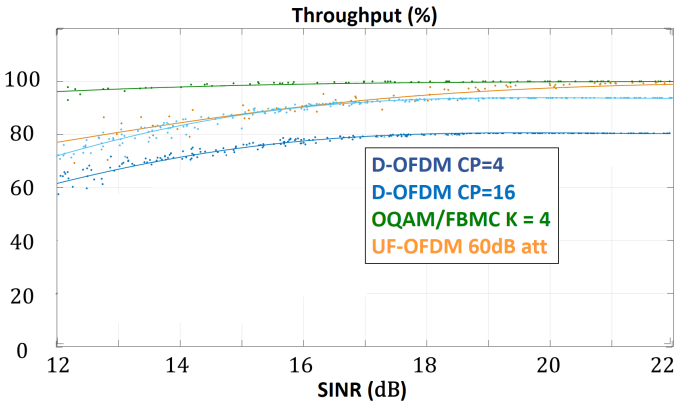

Fig. 5. Throughput performance with respect to the signal-to-interference-plus-noise ratio.

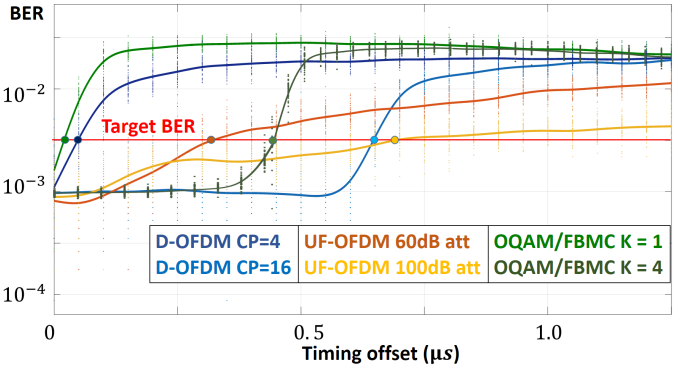

Fig. 6. BER performance with respect to the timing offset. The target BER determines the highest tolerable timing offset.

are the transmitters and car #2 is the receiver. Car #1 and car #3 transmit in the same carrier frequency but on two distinct non-overlapping sub-bands (upper and lower, with 24 data carriers each). It is assumed that car #2 perceives car #1 transmission perfectly synchronized and car #3 transmission with a certain timing offset. The timing offset is adjusted in 50 ns steps, which correspond to a degree of unsynchronization of 1 sample. Figure 6 shows the BER performance with respect to this timing offset, where the target BER determines the highest tolerable timing offset. Note that, in case of OFDM, if car #3 transmission is misaligned, then its timing offset is equal to the relative delay to car #2. When the FFT operation is performed, car #2 may experience ISI and ICI from car #3 because, if the OFDM symbol of car #3 does not lie within the FFT window of car #2 the FFT duration may be extended over the symbol boundary, and if the OFDM symbol of car #3 lies within the FFT window, then it will be now less robust to the delay spread of the channel. Note that the ISI and ICI from car #3 cause performance degradation also to car #1 transmission, which is perfectly synchronized. This multiple timing-offsets issue in OFDM may be solved by increasing the CP duration, so that it covers both the longest transmission delay and the channel's maximum delay spread. As shown in Figure 6, the receiver can absorb small positive timing offsets (signal arrives later than the receiver expected) as long as the timing offset remains within the duration of the CP, approximately. However, OFDM performance degrades significantly as soon as the timing error is such that the channel transient exceeds the CP duration. It is noteworthy that the experimental results of the effect of timing errors on OFDM are in concordance with [10].

On the other hand, as shown in Figure 6, OQAM/FBMC exhibits a similar behavior and the signal is protected as far as the robustness provided by the overlap factor is not surpassed. In contrast, any timing offset in UF-OFDM systems affects the system performance, since no CP is inserted. Even with a small timing offset, the orthogonality between subcarriers is destroyed, which causes ICI, and ISI. However, for UF-OFDM the filter ramp-up and ramp-down may provide a soft protection against timing offset, since relatively small energy is contained, and as shown the degradation instead of sudden is progressive. This type of protection is also applicable to OQAM/FBMC, although the results shown in Figure 6 do not implement this mechanism.

Finally, Figure 7 shows the throughput performance comparison of SISO and MIMO 2x2 with respect to the SINR. In this case, the transmitter and receiver boards are located 1 m apart. The transmitter uses spatial multiplex (open loop/CSIR) MIMO with no precoding and, because of the distance, a sparse multipath channel is expected during the experiments. In order to achieve competitive MIMO results, OQAM/FBMC pilots are implemented according to [21]. The impact of the CP on the throughput is also present and, as shown, for higher values of SINR the performance of UF-OFDM is slighthly better than that of OQAM/FBMC.

VII. Conclusions

The hardware testbed presented in this paper is a valid framework for rapid physical layer prototyping, allowing arbitrary combinations of single and multi-antenna transmit and receive nodes. Although implementing an OFDM waveform

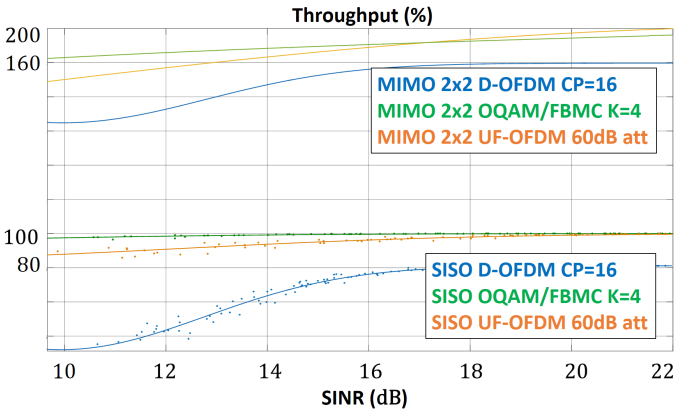

Fig. 7. Throughput performance comparison of SISO and MIMO 2x2 with respect to the signal-to-interference-plus-noise ratio in a MIMO.

is less complex, results show that OFDM is less robust against the lack of synchronization. However, there exist mechanisms that improve OFDM robustness (e.g. increasing the length of the CP or filtering, i.e. UF-OFDM). On the other hand, OQAM/FBMC is more robust against the lack of synchronization, but not as easily applicable to MIMO, since straightforward implementations of FBMC are more complex than OFDM. UF-OFDM is also robust against timing issues and has a complexity similar to OFDM. In any case, we have highlighted the need for a software defined radio approach to provide more flexibility to accommodate sidelink communication into a frame-structured cellular system.

Future work shall use the testbed to research the impact of mobility on the performance of FBMC, UF-OFDM (as well as other waveforms investigated by METIS-II) and check their degradation, including a performance assessment when different modifications to the numerology of the waveforms are tested. Moreover, additional efforts should be made in order to harmonize the PHY layer with a single transmission chain that could implement a set of different waveforms.

ACKNOWLEDGMENT

Part of this work has been performed in the framework of the H2020 project METIS-II (H2020-ICT-2014-2, topic ICT-14-2014) co-funded by the European Commission. The authors would like to acknowledge the contributions of their colleagues. The views expressed are those of the authors and do not necessarily represent the project. Part of this work has been also supported by the Ministerio de Economia y Competitividad, Spain (TEC2014-60258-C2-1-R), by the European FEDER funds.

REFERENCES

[1] "Part 11: Wireless LAN Medium Access Control (MAC) and Physical Layer (PHY) Specifications Amendment 6: Wireless Access in Vehicular Environments" (PDF). IEEE 802.11p published standard. IEEE. July 15, 2010. Retrieved August 10, 2011.

[2] D. Martín-Sacristán, J. F. Monserrat, J. Cabrejas-Peñuelas, D. Calabuig, S. Garrigas, and N. Cardona, "On the way towards fourth-generation mobile: 3GPP LTE and LTE-advanced," *EURASIP Journal on Wireless Communications and Networking*, 2009.

[3] P. Siohan, C. Siclet, and N. Lacaille, "Analysis and Design of OFDM/OQAM Systems Based on Filterbank Theory," *IEEE Transactions on Signal Processing*, vol. 50, no. 5, pp. 1170-1183, August 2002.

[4] V. Vakilian, T. Wild, F. Schaich, S. Ten Brink, and J.-F. Frigon, "Universal-filtered multi-carrier technique for wireless systems beyond LTE," *in IEEE Globecom Workshops (GC Wkshps)*, 2013, pp. 223228.

[5] G. Jue, S. Shin, Keysight Technologies *Implementing a Flexible Testbed for 5G Waveform Generation and Analysis,* White Paper, Keysight Technologies, Apr. 20, 2015.

[6] M. Danneberg, R. Datta and G. Fettweis, "Experimental Testbed for Dynamic Spectrum Access and Sensing of 5G GFDM Waveforms," *Vehicular Technology Conference (VTC Fall), 2014 IEEE 80th*, Vancouver, BC, 2014, pp. 1-5.

[7] F. Kaltenberger, R. Knopp, M. Danneberg and A. Festag, "Experimental analysis and simulative validation of dynamic spectrum access for coexistence of 4G and future 5G systems," *Networks and Communications (EuCNC), 2015 European Conference on,* Paris, 2015, pp. 497-501.

[8] K. W. Martin, "Small side-lobe filter design for multitone data-communication applications," in *IEEE Transactions on Circuits and Systems II: Analog and Digital Signal Processing*, vol. 45, no. 8, pp. 1155-1161, Aug 1998.

[9] M. Bellanger, *FBMC physical layer: a primer*, PHYDYAS, Jan 2010.

[10] Y. Mostofi and D. C. Cox, "Mathematical analysis of the impact of timing synchronization errors on the performance of an OFDM system," in *IEEE Transactions on Communications*, vol. 54, no. 2, pp. 226-230, Feb. 2006.

[11] M.AA Hasan, F. Nabita, A, Khandakar, I. Ahmed, F. Ahmed, "Analytical Evaluation of Timing Offset Error in OFDM System," *Communication Software and Networks,* vol.3, no.7, pp.26-28, Feb. 2010.

[12] H. Saeedi-Sourck, Y. Wu, J. W. M. Bergmans, S. Sadri, B. Farhang-Boroujeny, "Sensitivity analysis of offset QAM multicarrier systems to residual carrier frequency and timing offsets," *Signal Process.* 91 (July (7)) (2011) pp. 16041612.

[13] H. Lin, M. Gharba, P. Siohan, "Impact of time and carrier frequency offsets on the FBMC/OQAM modulation", *Signal Processing*, vol. 102, pp. 151–162, 2014.

[14] T. Fusco, A. Petrella and M. Tanda, "Sensitivity of multi-user filter-bank multicarrier systems to synchronization errors," *Communications, Control and Signal Processing, 2008. ISCCSP 2008. 3rd International Symposium on,* St Julians, 2008, pp. 393-398.

[15] X. Wang, T. Wild and F. Schaich, "Filter Optimization for Carrier-Frequency- and Timing-Offset in Universal Filtered Multi-Carrier Systems," *Vehicular Technology Conference (VTC Spring), 2015 IEEE 81st,* Glasgow, 2015, pp. 1-6.

[16] Q. Bai and J. A. Nossek, "On the effects of carrier frequency offset on cyclic prefix based OFDM and filter bank based multicarrier systems," *Signal Processing Advances in Wireless Communications (SPAWC), 2010 IEEE Eleventh International Workshop on,* Marrakech, 2010, pp. 1-5.

[17] A. Aminjavaheri, A. Farhang, A. RezazadehReyhani, B. Farhang-Boroujeny, "Impact of Timing and Frequency Offsets on Multicarrier Waveform Candidates for 5G", arXiv:1505.00800v2 [cs.IT] 9 Sep 2015 [Online]. Available: http://arxiv.org/abs/1505.00800 [Last accessed: March 23, 2016].

[18] Mango Communications, "WARP v3 Kit", [Online]. Available: https://mangocomm.com/products/kits/warp-v3-kit, [Last accessed: March 21, 2016].

[19] T. M. Schmidl, D. C. Cox, "Robust Frequency and Timing Synchronization for OFDM," *IEEE Transactions on Communications,* vol. 45, no. 12, pp. 16131621, Dec. 1997.

[20] C. Dick and F. Harris, "FPGA implementation of an OFDM PHY," in *Proc. Conference Record of the Thirty-Seventh Asilomar Conference on Signals, Systems and Computers.,* vol. 1, Nov. 2003, pp. 905 909.

[21] J.-P. Javaudin, D. Lacroix, A. Rouxel, "Pilot-aided channel estimation for OFDM/OQAM," in *Vehicular Technology Conference, 2003. VTC 2003-Spring. The 57th IEEE Semiannual* , vol.3, no., pp.1581-1585 vol.3, 22-25 April 2003.